Development of a Mathematical Model for Apple Juice Compounds Rejection in a Spiral-wound Reverse Osmosis Process

Al-Obaidi M. A., Kara-Zaïtri C. and Mujtaba I. M. *

School of Engineering, Faculty of Engineering and Informatics. University of Bradford, Bradford, West Yorkshire BD7 1DP, UK

***Corresponding author, Tel.: +44 0 1274 233645**

E-mail address: I.M.Mujtaba@bradford.ac.uk

Abstract

The use of Reverse Osmosis (RO) membrane processes for the clarification and the concentration of apple juice is proposed as an alternative to the conventional concentration technique, which is based on evaporation and freezing. Several models have been published on RO process models relying on different assumptions that predict the permeate flux and aroma compounds rejections for aqueous solutions apple juice. The solution-diffusion model (Lumped model) has been applied for the previous models. The main instrument of this study is the use of the gPROMS software to develop a new distributed steady state model that will relax a number of earlier assumptions.

The model has been validated with an observational data of apple juice filtration derived from the literature by analysing the permeate flux and the performance of membrane rejection at different concentrations, temperatures and pressures for a laboratory scale of spiral-wound RO module. Simulated results corroborate with experimental and model predictions.

***Keywords*:** Apple Juice Concentration; Spiral-wound Reverse Osmosis; One Dimensional Distributed Model; gPROMS software.

1. Introduction

The concentration of fruit juices is achieved by reducing the water content. This has many advantages, including easier and cheaper conservation, storage, transportation and distribution of the extracted juice. Conventional methods of fruit juices concentration are usually conducted using a high temperature multi-stage vacuum evaporation process. This process usually results in significant losses of nutritional compounds, such as vitamin C, as well as associated thermal effects (Pozderovic´ et al. 2006). As a result, RO has become an alternative process to the conventional methods for removing water from fruit juices and other liquid foods (Girard and Fukumoto, 2000). However, one of the main disadvantages of using RO is related to lower concentration of the yield in comparison to the thermal process due to high osmotic pressure limitation. Having said this, the RO process has affirmed its

potential as the prominent process for retaining the aroma compounds (Jiao et al., 2004). Therefore, the RO process is a well-recognized technique for concentrating aqueous solutions within a limit of 25 to 30 °Brix, which is quite below the typical value of 45 to 60 °Brix gain by the evaporation process (Pepper, 1990). With the aim to improve the concentration and yet retain the critical aroma feature, this research proposes a RO process but one that is used as a pre-concentration step with other technologies (Sheu and Wiley, 1983).

Due to the obvious high commercial implications, several attempts can be found in the literature to improve the concentration of apple juice. Many such models are based on the RO process in order to measure permeate flux and to elucidate the rejection of one component and multi-component fruit solutions. A critique on the current literature is discussed in the following section.

Nabetani et al. (1992a) have proposed a new correlation to estimate the osmotic pressure of sucrose and glucose solution using thermodynamic definition of the osmotic pressure. The proposed equations assume that the osmotic pressure can be expressed in terms of solute concentration. Accordingly, Nabetani et al. (1992b) have developed a model using the combination of sucrose and glucose osmotic pressure developed in Nabetani et al. (1992a) with the solution-diffusion model equations. The model can predict the permeation of apple juice solution considering the solution physical properties of both one component and a binary solute solution. The model has been validated for a tubular RO module type (ZF 99) supplied by PCI (Paterson Candy International, England) and shows a good agreement between experimental RO data and those calculated on the basis of the solution-diffusion model. However, this particular model considered only sucrose and glucose solute concentration in the bulk retentate with ignored the permeate concentration.

Álvarez et al. (1997) have used the solution-diffusion model and the film theory with the proposed osmotic pressure of Nabetani et al. (1992b) to predict the permeate flux in apple juice concentration. This was done by using a tubular polyamide RO membrane type (AFC 99) supplied by PCI (Paterson Candy International, England). The model incorporates the physico-chemical correlations to evaluate the characteristics of concentrated apple juice. However, the model ignored the solute concentration at the permeate side and degraded the osmotic pressure caused by fructose and sorbitol in spite of taking into account the contribution of sucrose, glucose and malic acid to the osmotic pressure. Furthermore, Álvarez et al. (1998) used the procedure developed by Matsuura et al. (1974) to calculate the solute

transport parameter for each aroma compound for a spiral-wound RO aromatic polyamide membrane type (MSCB 2521 R99) supplied by Separem Spa. (Biella, Italy). Table 1 reports the values of free energy parameter, steric Taft number and solute transport parameter for each aroma compound. Then, the solution-diffusion model is used to estimate the rejection of hydrophilic aroma compounds by considering the average value of inlet feed and retentate as the concentration of bulk solution, but overlooked the osmotic pressure. After that, Álvarez et al. (2001) studied the rejection of aroma compounds using experimental data of solute transport parameter for each aroma compounds calculated for the same above module of RO membrane in the solution-diffusion model. Similarly, this work shows the influence of temperature and feed flow rate on pure water permeability coefficient. The model studied was used to predict the impact of operating conditions such as feed flow rate and concentration on the permeate flux and aroma compound rejections. However, feed osmotic pressure is referred only to glucose.

Álvarez et al. (2002) have used the same procedure developed in the work shown above to predict the aroma compounds rejection and the permeate flux during the reverse osmosis concentration of apple juice at laboratory and pilot-scales of MSCB 2521 R99 and MSCE 4040 R99 spiral wound membrane supplied by Separem Spa. (Biella, Italy) respectively. The model can predict the influence of operating conditions on permeate flux and aroma compounds rejection. However, this work not only ignored the contribution of fructose and sorbitol in feed osmotic pressure, but also neglected the concentration at the permeate side.

To the best of authors' knowledge, all the published RO process modelling for the concentration of apple juice has been carried out using the entire arrangement as a black box and simply taking average inputs and outputs parameter values. In this paper, the finite difference approach is used instead as it gives more accurate results because it takes into account the variation of the operating parameters along the entire system. Also, the above studies have been proposed to describe flux behaviour and compounds retention by relying on the assumption that the osmotic pressure of sugar is only caused by glucose, sucrose and malic acid, and thus ignoring fructose and sorbitol. Pereira et al. (1976) confirmed that glucose and fructose have greater mass transfer and solute transport characteristics than that of sucrose. To systematically resolve this problem, the scope of this paper is to present the development of a distributed one dimensional steady state model and define and asses the variation of the operating conditions as a function of position along the x-axis of the spiral-wound module in the process of apple juice filtration. As well as this, the contribution of all

sugar species in the feed osmotic pressure will be taken into consideration. The validation of this model will be based on a comparison between simulation and experimental results derived from the literature. The process model developed can be used later to assess the operating conditions and system design in order to optimize the concentration of apple juice and the retention of aroma compounds.

2. The Main Principles

Reverse Osmosis can be defined as a process of removing undesirable species (salts, pollutants, etc.) from liquid solutions (seawater, wastewater, etc.) by pumping the solution at a hydraulic pressure greater than the osmotic pressure within a closed vessel to move water from high solute side to the diluted side (Jain et al., 2004). There does not appear to be a widespread agreement on the mechanisms of water and solute transport through RO membrane for aqueous solutes (Girard and Fukumoto, 2000). However, the most accepted approaches in this respect are the Solution-diffusion and Preferential sorption theories. The first theory assumes that solvent and solute dissolve in the membrane and pass through by diffusion, while the second theory assumes that solvent and solute are adsorbed at the membrane surface and then pass through the membrane pores.

Generally, as the water is removed and the solute is rejected and accumulated at the membrane surface, the water flux drops due to an increase in the osmotic pressure of the feed and concentration polarization impact. There are considered as the main factors causing flux deterioration. These impediments can be fixed by altering the operating condition such as, feed pressure, concentration, temperature and cross-flow velocity and also by turbulence promotion, back flushing/washing and pulsed flow.

Normally, a solution treated by RO in food industries is considered as a multi-component solution, which contains a number of solutes at different concentrations. Specifically, apple juice comprises two groups of organic compounds; sugar and aroma compounds, which are categorized as esters (the main compound), aldehydes and alcohols. Also, aroma is one of the most appreciated fresh fruit juice flavor characteristics and is of great importance by consumers. Aroma is due to a large number of volatile organic compounds present in different concentrations, which play a key role in customer perception and satisfaction (Cheong et al., 2010).

2. Materials and Methods

2.1 Apple Juice Characteristics

Table 1 shows the composition and concentration of the apple juice (sugar and aroma compounds) used by Álvarez et al. (2002) in all of the experiments as the feed with concentration 10.5± 0.5 °Brix. The solution was prepared from 72 °Brix concentrated apple juice supplied by the apple processing company Valle, Ballina and Férnandez, S. A. (Villaviciosa, Spain), by adding distilled water.

2.2 Membrane Module Characteristics and Operating Conditions

The RO system used in all of the experiments conducted by Álvarez et al. (2002) was designed in a laboratory scale experiment consisting of a MSCB 2521 R99 spiral-wound aromatic polyamide membrane module supplied by Sparem Spa. (Biella, Italy). The detail of the manufacturer's specification membrane module is presented in Table 2. Experiments are carried out using a batch operation mode where the standard flow configuration of the feed volume is plug flow (passes once time through the system) and the concentrate retentate is recycled back to the feed tank to achieve high system recovery. In addition, permeate was recycled back to the feed tank to maintain a constant concentration and then removed from the equipment which concentration was increased. Experiments are implemented at three different trans-membrane pressures of 14.8, 24.673 and 34.542 atm within 20 to 30 °C , while the used inlet feed flow rate are 5.5556E-5, 1.111E-4 and 1.6667E-4 m^3/s respectively.

3. Model Rationale and Development

3.1 Assumptions

A number of reasonable assumptions and simplifications are used in order to develop this model. They include:

1. The module is made up of porous flat sheet with spacers and negligible leaf curvature.
2. Validity of the solution-diffusion model for the transport of the solvent and solutes through the membrane.

3. Validity of the Darcy's law for the feed and permeate channels, which assumes that the pressure drop is proportional to the feed and permeate flow rate and the friction parameter is applied to characterize the pressure drop.
4. Validity of the film model theory to estimate the concentration polarization impact.
5. The feed osmotic pressure is caused by the impact of all the species found in sugar and not restricted to only sucrose, glucose and malic acid.
6. Constant pressure of 1 atm on the permeate side.
7. Complete mixing in the y-axis of the feed channel due to the existence of a network of spacers.
8. The underlying process is assumed to be isothermal.

3.2 Model Structure

A computational one dimensional model was developed in this study to predict the variation of operating parameters and permeate flux in the x-axis during the reverse osmosis concentration of apple juice at laboratory scale spiral-wound RO process.

The details of model development, the equations and the physic-chemical properties of apple juice used throughout the simulation study are described below.

Based on Assumption 2, the solution-diffusion model is valid to predict the permeate flux through the membrane at any point along the x-axis as expressed by the following equation (Lonsdale et al., 1965).

$$J_{w(x)} = A_w \left(\Delta P_{b\,(x)} - \Delta \pi_{Total,(x)} \right) \quad (1)$$

A_w, $J_{w(x)}$ (m/s, m/ s atm) are the water flux at any point along the x-axis and the membrane permeability coefficient respectively. A_w was experimentally determined for the spiral-wound module type (MSCB 2521 R99) using pure water and accounts for the pore distribution of the membrane, porosity and membrane thickness. Álvarez et al. (2001) introduce the following correlation to show the impact of feed flow rate and operating temperature on A_w.

$$A_{w,\,T_b} = 9.059x10^{-7} \left(\frac{T_b}{25}\right)^{0.62} \left(\frac{36.0x10^5\, F_{b(0)}}{400}\right)^{-0.1447} \quad (2)$$

The above equation confirms that the water permeability coefficient slightly decreased with inlet feed flow rate and increased with temperature.

192 ($\Delta P_{b(x)} - \Delta\pi_{Total,(x)}$) is the quantity of force per unit area required to handle the osmotic
193 pressure and release pure water from the feed solution. $\Delta P_{b(x)}$ (atm) is the trans-membrane
194 pressure defined in Eq. (3).

195 $$\Delta P_{b\,(x)} = \left(P_{b(x)} - P_p\right) \quad (3)$$

196 $P_{b(x)}$, P_p are the feed pressure at any point along the x-axis and the constant permeate pressure
197 (Assumption 6) respectively. While, the overall trans-membrane pressure (TMP) (atm) for
198 each run is calculated as:

199 $$TMP = \frac{P_{b(0)} + P_{b(L)}}{2} - P_p \quad (4)$$

200 Where $P_{b(0)}$ and $P_{b(L)}$ (atm) are the pressure into the membrane and the pressure at the outlet
201 of the membrane respectively.
202 Because the aroma compounds concentration is very small compared to the sugar compounds
203 in apple juice (Table 1), $\Delta\pi_{Total,(x)}$ can only refer to the summation of the osmotic pressure
204 difference of sugar compounds along the length of the membrane. The osmotic pressure
205 difference of each sugar species can be defined as:

206 $$\Delta\pi_{(x)} = \pi_{Cw(x)} - \pi_{Cp(av)} \quad (5)$$

207 $\pi_{Cw(x)}$, $\pi_{Cp(av)}$ (atm) are the osmotic pressure of any sugar compound at the membrane wall
208 and permeate channel respectively.
209 Eq. (5) can be written as:

210 $$\Delta\pi_{(x)} = R\,T_b\left(C_{w(x)} - C_{p(av)}\right) \quad (6)$$

211 C_w and $C_{p(av)}$ (kmol/m³) are the solute concentration of sugar or aroma compounds at any
212 point along the x-axis at the membrane wall and average solute concentration at the permeate
213 side respectively. Also, R, T_b (atm L/K mol, K) are the gas constant and the apple juice
214 temperature respectively.
215 The solute flux $J_{s(x)}$ (kmol/m² s) of any sugar or aroma compounds along the x-axis can be
216 calculated as:

217 $$J_{s(x)} = B_s\left(C_{w(x)} - C_{p(av)}\right) \quad (7)$$

218 B_s (m/s) is the solute transport parameter of the determined species (sugar or aroma), which
219 is assumed as a constant along the length of the membrane and treated as unknown
220 parameters.
221 The solute flux is lower than volumetric solvent flux, and so $J_{s(x)}$ can be expressed as:

222 $$J_{s(x)} = J_{w(x)}\,C_{p(av)} \quad (8)$$

Eq. (6) can be written as:

$$\Delta\pi_{(x)} = R\,T_b\,\frac{J_{s(x)}}{B_s} \quad (9)$$

Substituting Eq. (8) in Eq. (9) and combining the result in Eq. (1) with re-arrangements yields to Eq. (10).

$$J_{w(x)} = \frac{A_w\,B_s\,\Delta P_{b(x)}}{B_s + A_w\,R\,T_b\,C_{p(av)}} \quad (10)$$

Based on Assumption 6, Eq. (11) can readily be derived as:

$$\frac{d\,\Delta P_{b(x)}}{dx} = \frac{d\,P_{b(x)}}{dx} \quad (11)$$

Following on, Darcy's law can be used to express the feed pressure drop along the x-axis according to Assumption 3.

$$\frac{dP_{b(x)}}{dx} = -b\,F_{b(x)} \quad (12)$$

$F_{b(x)}, b$ (m³/s, atm s/m^4) are the feed flow rate at any point along the x-axis and the friction parameter respectively. Taking the total mass balance based on the flow rate, gives:

$$F_{b(0)} = F_{b(x)} + F_{p(x)} \quad (13)$$

$F_{b(0)}, F_{p(x)}$ (m³/s) are the inlet feed flow rate and the permeate flow rate respectively. Also, taking the total mass balance across a small section in the feed channel of the unit gives:

$$\frac{dF_{b(x)}}{dx} = -\,W\,J_{w(x)} \quad (14)$$

W (m) is the width of the membrane.

Furthermore, taking the derivative of Eq. (13) yields Eq. (15) to express the variation of permeated flow rate along the x-axis as:

$$\frac{dF_{b(x)}}{dx} = -\frac{dF_{p(x)}}{dx} = W\,J_{w(x)} \quad (15)$$

Now, Dividing Eq. (12) and Eq. (14), yields:

$$\frac{d\,\Delta P_{b(x)}}{dF_{b(x)}} = \frac{b\,F_{b(x)}}{W\,J_{w(x)}} \quad (16)$$

The above equation can be written in the form of Eq. (17) by putting the value of solvent flux from Eq. (10).

$$F_{b(x)}\,dF_{b(x)} = \frac{W\,A_w\,B_s\,\Delta P_{b(x)}}{b\,(B_s + A_w\,R\,T_b\,C_{p(av)})}\;d\Delta P_{b(x)} \quad (17)$$

Further simplification, yields the following expression:

$$F_{b(x)}\,dF_{b(x)} = \emptyset\;\Delta P_{b(x)}\,d\Delta P_{b(x)} \quad (18)$$

Where, $$\emptyset = \frac{W\,A_w\,B_s}{b\,(B_s + A_w\,R\,T_b\,C_{p(av)})} \quad (19)$$

$\emptyset$ is a parameter that can be calculated for all the sugar and aroma compounds and then the average value will be considered as $\emptyset_{(\mathrm{mix})}$ for the rest of calculations.

$$\emptyset_{(mix)} = \frac{\sum_{i=1}^{n} \frac{W\, A_W\, B_S}{b\left(B_S + A_W\, R\, T_b\, C_{p(av)}\right)}}{n} \quad (20)$$

where, n = Total number of sugar and aroma compounds

Re-arrangement with integration of Eq. (18) gives a correlation to calculate the feed flow rate at any point along the x-axis as follows:

$$F_{b(x)} = F_{b(0)} + \emptyset_{(mix)}^{0.5} \left(\Delta P_{b_{(x)}} - \Delta P_{b_{(0)}} \right) \quad (21)$$

Substituting Eq. (21) into Eq. (12) and taking the integration facilitates the calculation of the trans-membrane pressure in any point along the x-axis.

$$\Delta P_{b(x)} = \Delta P_{b(0)} - b\, x\, F_{b(0)} - b\, x\, \Delta P_{b(x)} \left(\emptyset_{(mix)}\right)^{0.5} + b\, x\, \Delta P_{b(0)} \left(\emptyset_{(mix)}\right)^{0.5} \quad (22)$$

Substituting Eqs. (20) and (22) into Eq. (10) with re-arrangement gives:

$$J_{w(x)} = \frac{\emptyset_{(mix)}\, b}{W} \left(\Delta P_{b(0)} - b\, x\, F_{b(0)} - b\, x\, \Delta P_{b(x)} \left(\emptyset_{(mix)}\right)^{0.5} + b\, x\, \Delta P_{b(0)} \left(\emptyset_{(mix)}\right)^{0.5} \right) \quad (23)$$

Also, another equation for solvent flux can be derived by taking the derivative of Eq. (11) with respect to the x-axis as follows:

$$\frac{dJ_{w(x)}}{dx} = \frac{\emptyset_{(mix)}\, b}{W} \left(\frac{d\Delta P_{b(x)}}{dx} \right) \quad (24)$$

Substituting Eq. (12) into Eq. (24) gives:

$$\frac{dJ_{w(x)}}{dx} = \frac{\emptyset_{(mix)}\, b}{W} \left(-b\, F_{b(x)} \right) \quad (25)$$

Then, the variation of solvent flux in the x-axis can be calculated by the following equation:

$$J_{w(x)} = J_{w(0)} - \left(\frac{\emptyset_{(mix)}}{W}\, b^2\, x\, F_{b(0)} \right) + \left(\frac{{\emptyset_{(mix)}}^2\, b^3}{W}\, \Delta P_{b(0)} \left(\frac{x^2}{2} \right) \right) - \left(\frac{{\emptyset_{(mix)}}^2\, b^4}{W}\, F_{b(0)} \left(\frac{x^3}{6} \right) \right) -$$

$$\left(\frac{{\emptyset_{(mix)}}^{2.5}\, b^4}{W}\, \Delta P_{b(x)} \left(\frac{x^3}{6} \right) \right) + \left(\frac{{\emptyset_{(mix)}}^{2.5}\, b^4}{W}\, \Delta P_{b(0)} \left(\frac{x^3}{6} \right) \right) \quad (26)$$

Where, $J_{w(0)}$ (m/s) is the water flux at the inlet edge of the membrane.

Here, it is assumed that the osmotic pressure is caused by the impact of all the species found in sugar (Assumption 5) in contrary to the statement of Álvarez et al. (2001) who neglects both fructose and sorbitol. Therefore, the solvent flux at x = 0 is calculated using Eq. (27) regarding the osmotic pressure, which is caused by sugar compounds (sucrose, glucose, malic acid, fructose and sorbitol).

$$J_{w(0)} = A_w \left(\Delta P_{b_{(0)}} - \left(\pi_{su(0)} + \pi_{g(0)} + \pi_{m(0)} + \pi_{f(0)} + \pi_{so(0)} \right) \right) \quad (27)$$

Where, $\pi_{su(0)}, \pi_{g(0)}, \pi_{m(0)}, \pi_{f(0)}$ and $\pi_{so(0)}$ are the osmotic pressure (atm) of sucrose, glucose, malic acid, fructose and sorbitol respectively. The estimation of the osmotic pressure caused by sucrose, glucose and malic acid at any point along the x-axis is carried out using the empirical equation derived by Nabetani et al. (1992b) as can be seen in Eq. (28).

$$\pi_{su(x)} + \pi_{g(x)} + \pi_{m(x)} = -\frac{R\,T_b}{V_w}\, ln\left\{\frac{\left[\frac{\left(1000-C_{w(su)(x)}-C_{w(g)(x)}\right)}{M_{ww}}\right]-\left[\frac{\left(4\,C_{w(su)(x)}\right)}{M_{su}}\right]-\left[\frac{\left(2\,C_{w(g)(x)}\right)}{M_g}\right]}{\left[\frac{\left(1000-C_{w(su)(x)}-C_{w(g)(x)}\right)}{M_{ww}}\right]-\left[\frac{\left(4\,C_{w(su)(x)}\right)}{M_{su}}\right]-\left[\frac{\left(2\,C_{w(g)(x)}\right)}{M_g}\right]}\right\} + \frac{R\,T_b\;C_{w(m)(x)}}{M_m} \quad (28)$$

While, the contribution of fructose and sorbitol to osmotic pressure is calculated by Eqs. (29) and (30).

$$\pi_{f(x)} = \frac{R\,T_b\,C_{w(f)(x)}}{M_f} \quad (29)$$

$$\pi_{so(x)} = \frac{R\,T_b\,C_{w(so)(x)}}{M_{so}} \quad (30)$$

Note, all the concentrations expressed in Eqs. (28), (29) and (30) are referred to the concentration of the species at the wall membrane and expressed in (kg/m³).

The concentration of the sugar and aroma compounds at the wall membrane was estimated based on Assumption 4, which in turn is based on the validity of the film model theory where the solvent flux is linked to concentration polarization and mass transfer coefficient, k by the following equation:

$$\frac{\left(C_{w(x)}-C_{p(av)}\right)}{\left(C_{b(x)}-C_{p(av)}\right)} = exp\left(\frac{J_{w(x)}}{k_{(x)}}\right) \quad (31)$$

$C_{b(x)}$, $k_{(x)}$ (kmol/m³, m/s) are the concentration in the feed channel of any species and the mass transfer coefficient respectively.

The feed velocity along the x-axis $U_{b(x)}$ (m/s) is calculated by:

$$U_{b(x)} = \frac{F_{b(x)}}{W\,t_f} \quad (32)$$

The feed pressure equation can be derived from integration of Eq. (12).

$$P_{b(x)} = P_{b(0)} - \left[b\,F_{b(0)}\,x\right] + \left[\emptyset_{(mix)}\,b^2\,\left(\frac{x^2}{2}\right)\,\Delta P_{b(0)}\right] - \left[\emptyset_{(mix)}\,b^3\,F_{b(0)}\left(\frac{x^3}{6}\right)\right] - \left[{\emptyset_{(mix)}}^{1.5}\,b^3\,\Delta P_{b(x)}\left(\frac{x^3}{6}\right)\right] + \left[{\emptyset_{(mix)}}^{1.5}\,b^3\,\Delta P_{b(0)}\left(\frac{x^3}{6}\right)\right] \quad (33)$$

The sugar or aroma compounds concentration at the feed channel and at any point along the x-axis is calculated using Eq. (34) as proposed by Lee et al. (2010).

$$\frac{d\frac{\left(C_{b(x)}\,F_{b(x)}\right)}{t_f\,W}}{dx} = -\frac{J_{w(x)}\,C_{p(av)}}{t_f} + \frac{J_{w(x)}\,C_{b(x)}}{t_f} + \frac{d}{dx}\left(D_{(x)}\,\frac{dC_{b(x)}}{dx}\right) \quad (34)$$

Then, substituting Eq. (31) and Eq. (8) into Eq. (7) with re-arrangement gives a correlation to calculate the concentration of any sugar or aroma compound at the permeate side. This equation will be used twice at x=0 and x=L as can be shown in Eqs. (35) and (36), and the average solute permeate concentration $C_{p(av)}$ (kmol/m³) is calculated using Eq. (37) as follows:

$$C_{p(0)} = \frac{B_s\, C_{b(0)}\ e^{\frac{J_{w(0)}}{k_{(0)}}}}{J_{w(0)} + B_s\ e^{\frac{J_{w(0)}}{k_{(0)}}}} \quad (35)$$

$$C_{p(L)} = \frac{B_s\, C_{b(L)}\ e^{\frac{J_{w(L)}}{k_{(L)}}}}{J_{w(L)} + B_s\ e^{\frac{J_{w(L)}}{k_{(L)}}}} \quad (36)$$

$$C_{p(av)} = \frac{C_{p(0)} + C_{p(L)}}{2} \quad (37)$$

The volumetric permeated flow rate along the x-axis in the permeate channel can be calculated using Eq. (38):

$$F_{p(x)} = W \int_{x=0}^{x=L} J_{w(x)}\, dx \quad (38)$$

Also, the model facilitates the evaluation of the performance of the unit by calculating the rejection of organic compounds as can be seen in the counter of Eq. (39).

$$Rej = \frac{C_{b(L)} - C_{p(av)}}{C_{b(L)}}\ x100 \quad (39)$$

The recovery of the module calculated using Eq. (40) is the fraction of the feed that is recovered as permeate at the permeate channel. Note that, for a laboratory scale apparatus, the permeate flow rate is small in comparison to feed flow rate.

$$Rec_{(Total)} = \frac{F_{p(Total)}}{F_{b(0)}}\ x100 \quad (40)$$

3.3 The Physical Properties Equations

The mass transfer coefficient is a function of pressure, concentration, flow rate and temperature, which means that k will vary with the membrane length. Schock and Miquel's (1987) correlation is used to estimate the mass transfer coefficient along the x-axis for any species of sugar or aroma compounds as can be depicted in Eq. (41).

$$k_{(x)} = 0.065 \left(\frac{D_{(x)}}{d_h}\right) Re_{b(x)}^{0.875}\ \ Sc_{(x)}^{0.25} \quad (41)$$

$D_{(x)}$, $Re_{b(x)}$, $Sc_{(x)}$ (m²/s, dimensionless) are the diffusion coefficient of any sugar or aroma compound, the Reynolds number and the Schmidt number of any sugar or aroma compound at any point along the x-axis respectively. The terms can be calculated as follows:

$$Re_{b(x)} = \frac{\rho_{b(x)}\, d_h\, U_{b(x)}}{\mu_{b(x)}} \quad (42)$$

$$Sc_{(x)} = \frac{\mu_{b(x)}}{\rho_{b(x)}\, D_{(x)}} \quad (43)$$

Where, $\rho_{b(x)}$, $\mu_{b(x)}$ and d_h (kg/m³, kg/m s, m) are the apple juice density, viscosity and the hydraulic diameter respectively.

The apple juice viscosity can be calculated as a function of concentration in °Brix and temperature using Eq. (44) (Constenla et al., 1989).

$$\frac{\mu_{b(x)}}{\mu_w} = exp\left(\frac{A\ °Brix_{(x)}}{100 - B\ °Brix_{(x)}}\right) \quad (44)$$

μ_w and $°Brix_{(x)}$ are the viscosity of water (8.94E-4 kg/m s) and the concentration of apple juice in °Brix. A and B are parameters related to the temperature and can be estimated using Eqs. (45) and (46).

$$A = -0.25801 + \frac{817.11}{T_b} \quad (45)$$

$$B = 1.8909 - 3.0212\ x10^{-3}\ T_b \quad (46)$$

T_b is the absolute temperature.

Eq. (47) can be used to calculate the variation of apple juice concentration in °Brix along the length of membrane regarding the concentration of the mixture in kg/m³.

$$°Brix_{(x)} = 0.099198\left(\sum_{i=1}^{n} C_{(x,n)}\right) \quad (47)$$

where, n = Total number of sugar and aroma compounds

Where, $C_{(x)}$ (kg/m³) is the concentration of sugar and aroma compounds at any point along the x-axis and calculated using Eq. (48).

$$C_{(x,i)} = C_{b(x,i)}\ M_{wt\ (i)} \quad (48)$$

where, *i* represents the particular species of any sugar or aroma compounds

$M_{wt\ (i)}$ (kg/kmol) is the molecular weight of any species under consideration.

The apple juice density is calculated using Eq. (49) as a function of concentration in °Brix and temperature (Constenla et al., 1989).

$$\rho_{b(x)} = 0.8272 + 0.34708 \exp\left(0.01\ °Brix_{(x)}\right) - 5.479\ x10^{-4}\ T_b \quad (49)$$

Then, the diffusion coefficient for any sugar species $D_{SU(x)}$ (m²/s) and aroma compounds $D_{AR(x)}$ (m²/s) along the x-axis can be calculated using the empirical equation proposed by Gladdon and Dole (1953) as can be seen in Eqs. (50) and (51) respectively.

$$D_{SU(x)} = D_s\left(\frac{\mu_w}{\mu_{b(x)}}\right)^{0.45} \quad (50)$$

$$D_{AR(x)} = D_a \left(\frac{\mu_w}{\mu_{b(x)}}\right)^{0.45} \quad (51)$$

D_s, D_a (m^2/s) are referred to the diffusion coefficient of any species of sugar and aroma compounds respectively in a very dilute solution. These coefficients have been calculated using the proposed correlation of Wilke and Chang (1955).

$$D_a = \left(\frac{7.4\, x10^{-8}\, (2.6\, M_w)^{0.5}\, (T_b+273.15)}{(1000\, \mu_{b(x)})\, (1000\, V_{bp,A})^{0.6}}\right) x10^{-4} \quad (52)$$

The above equation is correlated to be compatible with the units used. M_w and $V_{bp,A}$ (kg/kmol, m^3/kmol) are the molecular weight of water and the molar volume of the solute at its normal boiling point. $V_{bp,A}$ values for all sugar and aroma compounds are shown in Table 1.

Finally, the model presented in this section is built within gPROMS (general Process Modelling System) Model builder, which provides a modelling platform for steady state and dynamic simulation, optimisation, experiment design and parameter estimation of any process.

4. Determination of Friction and Transport Parameters

4.1 Determination of Friction Parameter

Unknown friction parameter of the membrane elements and the operating conditions should be determined before solving the model equations. In the simulation study, experimental data will be used to predict the best values of unknown feed channel friction parameter. These are then used with the known parameters to assess the behaviour of the unit with the variance of operating variables.

In this work, the friction parameter has been estimated using an optimization methodology of the gEST parameter estimation tool developed in gPROMS (Process System Enterprise Ltd., 2001). This method has been used on the experimental data of Álvarez et al. (2002) in order to optimize the value of friction parameter. The starting point was based on an initial guess, which was subsequently used to solve the model equations. The preferred value of the friction parameter is reached by continuously varying the predicted value until close fit with experimental data is reached. The registered value of friction parameters for the membrane type MSCB 2521 R99 of effective area 1.03 m^2 is 90 (atm s/m^4).

4.2 Determination of Solute Transport Parameters

The solute flux of sugar and aroma compounds through the membrane is given by the product of solute transport parameter and the solute concentration difference at the two channels of the unit as expressed in Eq. (7). So, for calculation purposes, a separate value of the solute transport parameter is required for each species for multiple solutes feed.

4.2.1 Solute Parameters of Aroma Compounds

The solute parameters of aroma compounds B_s (m²/s) for the reverse osmosis module consisting of a spiral-wound aromatic polyamide membrane type (MSCB 2521 R99) were calculated using the equation of Álvarez et al. (2001).

$$B_{s\,i} = B_{s\,i,Ref.}\, exp^{0.098(T_b - T_{Ref.})} \tag{53}$$

i represents the particular species under consideration. $B_{s\,i}$, $B_{s\,i,Ref.}$ and $T_{Ref.}$ are the solute parameter of any aroma compounds at operating temperature (T_b) and the reference temperature of 25 °C ($T_{Ref.}$). Eq. (53) was obtained for a temperature range of 15 °C to 30 °C. The estimated values of solute parameter for each aroma compounds at 25 °C are shown in Table 1.

4.2.2 Solute Parameters of Sugar Compounds

The solute transport parameters B_s (m²/s) of sugar compounds were calculated using the correlation of Matsuura et al. (1976), which assumed the concept of free energy parameter ($-\Delta\Delta G/RT$) governing non-ionized polar organic solutes in aqueous solution reverse osmosis separation. Eq. (54) shows the general form of this correlation.

$$\ln B_{s\,i} = \ln C^*_{NaCl} + \left(-\frac{\Delta\Delta G}{RT}\right)_i + \delta^* Es^* \tag{54}$$

i represents the particular species under consideration. $\ln C^*_{NaCl}$ is a constant depending on the chemical nature of the membrane and the effective pore size where NaCl as the reference solute. While, the steric Taft number ($\delta^* Es^*$) is characteristic of each solute in the bulk solution and represents the properties of the solute on the membrane-solution interface and relates to the membrane type.

For the aromatic polyamide membrane type, Matsuura et al. (1976) have found the quantity $\ln C^*_{NaCl}$ using the experimental solute transport parameter data $B_{s\,NaCl}$ for a completely ionized inorganic solute taken NaCl as a reference, and the known values of ($-\Delta\Delta G/RT$) for both Na^+ and Cl^- ions as can be shown in Eq. (55).

$$\ln B_{s\,NaCl} = \ln C^*_{NaCl} + \left[\left(-\frac{\Delta\Delta G}{RT}\right)_{cation} + \left(-\frac{\Delta\Delta G}{RT}\right)_{anion}\right] \quad (55)$$

Then, the numerical value of (-ΔΔG/RT) for several monovalent inorganic cations and anions in aqueous solutions used in conjunction with aromatic polyamide membrane in reverse osmosis has been obtained using Eq. (56) (Matsuura et al., 1975; Dickson et al., 1975).

$$\ln B_{s\,NaCl} = \ln C^*_{NaCl} + \left[\left(-\frac{\Delta\Delta G}{RT}\right)_i\right] \quad (56)$$

While, the free energy parameter of each sugar species (-ΔΔG/RT) and the steric Taft number (δ^*Es^*) of each species of sugar has been calculated by Matsuura et al. (1976) and shown in Table 1.

Finally, the transport parameter for each species of sugar for the aromatic polyamide membrane type (MSCB 2521 R99) at 25 °C can be calculated using Eq. (54) as reported in Table 1. However, the transport parameter of malic acid was taken from Malalyandi et al. (1982).

5. Model Validation, Results and Discussion

The model described in Section 3 has been validated by comparing the model predictions results with those obtained from actual experimentation for a MSCB 2521 R99 spiral-wound RO aromatic polyamide membrane module carried out by Álvarez et al. (2002). The comparison between the model predictions and experiments is shown in the following section.

Figure 1 shows the model rejections of two selected aroma compounds, Isopentyl acetate and *trans*-2-hexanal at two different inlet feed flow rates versus the operating temperature and against experimental results. While, Figures 2 and 3 show the experimental and theoretical results of outlet water flux and feed flow rate versus the operating trans-membrane pressure for different inlet feed flow rates at operating temperature 20 °C.

The expectation that increasing inlet feed temperature would increase the solute rejection is validated here as it decreases the viscosity of apple juice as expressed in Eq. (44). This accelerates the flux of water through the membrane and reduces the concentration polarization impact. Interestingly, Figure 1 also shows a slight reduction of Isopentyl acetate and *trans*-2-hexanal rejections with operating temperature for different inlet feed flow rates. The probable explanation for this can be that by increasing the feed temperature, the solute concentration over the membrane wall will increase and causes an increase in solute flux accompanied by the penetrated water that causes an increase in the permeate solute

concentration at the permeate channel. As a result, the solute rejection will decrease as expressed in Eq. (39).

Furthermore, Figure 1 shows that the model tends to only underestimate the rejection of *trans*-2-hexanal at lower operating temperatures and inlet feed flow rate. This might be attributed to the inaccurate estimation of the transport membrane parameter of *trans*-2-hexanal at such conditions.

To illustrate the impact of operating trans-membrane pressure and inlet feed flow rate on solute rejection, Figure 2 shows the variation of Isopentyl acetate rejection versus the operating trans-membrane pressure at three different inlet feed flow rates with comparative data between the model and experiments results. It is expected that the retention of any species will increase due to the increase in operating pressure in turn due to an increase in the water flux passing the membrane. Moreover, the increase of the inlet feed flow rate causes an increase in the Isopentyl acetate rejection due to a reduction in solute flux through the membrane. The increased feed flow rate reduces the wall membrane concentration and causes a decrease of osmotic pressure along the membrane length. Also, an increase in the feed flow rate causes a specific impact on the solute retention by decreasing the amount of accumulated salt on the membrane wall. Consequently, the increasing applied pressure for the same inlet feed flow rate will increase the accumulated salt on the membrane by increasing the water flux.

Figure 3 illustrates the effect of operating pressure and inlet feed flow rate in the outlet water flux. The water flux increases due to increase in the operating pressure in line with Eq. (1), which shows that the feed pressure has a substantial impact by bringing up the diffusion rate of water passing through the membrane. Also, it can be noticed that the impact of the inlet feed flow rate is significantly greater at higher operating pressures due to a higher reduction in concentration polarization caused by combining the concurrent impacts of the two feed flow rate and pressure parameters.

Similarly, Figure 3 shows that the model predicts the water flux within an accepted error, except at high inlet feed flow rate and operating pressure. This is due to the use of a constant value of water permeability coefficient in all the calculations. It can be argued that this coefficient decreases exponentially with the operating trans-membrane pressure as a result to membrane compaction. At the same time, the water permeability coefficient increases due to an increase in the operating temperature, that causes a reduction in water viscosity. It is expected that these reasons contribute to the slight discrepancy between the outputs of the model and experiments at these conditions.

The clear corroboration with experimental data readily shows the suitability of the model to measure the observed retention and water flux parameters with an accepted error over the operating ranges of trans-membrane pressures and temperatures.

Figure 4 shows the consistence between the model prediction and experiments results for the outlet feed flow rate versus the operating trans-membrane pressure using three different inlet feed flow rates.

Figure 5 shows the effect of operating trans-membrane pressure in the outlet °Brix for different inlet feed flow rates. It is expected that the concentration in °Brix will increase due to an increase in the operating pressure. This is due to the increase in water flux by increasing the operating pressure. The concentration in °Brix that can be obtained is limited to the range 10.55 – 11.32 of used pressure and this might be attributed to the use of small specific area of membrane module.

It is also interesting to notice that the outlet concentration in °Brix is almost the same for all three inlet feed flow rates at lower inlet operating pressure. However, there is a noted discrepancy at higher operating pressures. Overall, the concentration in °Brix decreases due to an increase in the operating feed flow rate, especially when using higher operating pressures in spite of increasing water flux with increasing inlet feed flow rate, as more specifically illustrated in Figure 3. The reason for this phenomenon is that increasing inlet feed flow rate results in increasing the mass transfer coefficient and decreasing the concentration polarization. Also, the increased feed flow rate reduces the wall membrane concentration and causes a decrease of osmotic pressure, which is followed by decreasing sugar and aroma compounds concentration along the membrane due to a better mixing in the feed channel.

Figure 6 displays the variation of operating temperature within the permissible limits of the manufacturer's specifications of the module as a function of apple juice concentration measured in °Brix. It can be observed that the concentration increases as a result to increase in the operating temperature. In line with Eq. (2), the water permeability coefficient increases with increasing the operating temperature, which causes an increase in water flux that raises the apple juice concentration in the feed side.

Finally, a 10% maximum error agreement is obtained in a comparison between experimental and calculated rejection for all aroma compounds as presented in Figure 7. The relatively small discrepancy can be attributed to two reasons. Firstly, the actual experiments of Álvarez et al. (2002) is carried out using apple juice concentration of 11 °Brix not 10.5 °Brix.

Secondly, constant solute transport parameters of aroma compounds are used in the calculation of solute flux through the membrane as can be seen in Eq. (7).

Conclusions

A mathematical one dimensional steady model applicable for apple juice concentration process using a spiral-wound reverse osmosis process has been developed with a simulation study of permeate flux and aroma compounds rejection. The model can predict the variation of the feed flow rate, sugar and aroma compounds concentration in both the feed and permeate channels, membrane wall concentration, feed pressure and water and solute fluxes in each point along the membrane length. A number of differential equations have been developed based on the solution-diffusion model, which takes into account the impact of all sugar species in the calculation of osmotic pressure. Besides, the model estimates the physical properties of apple juice using the empirical equations that shows the impact of concentration and temperature derived from the literature. Also, the solute transport parameters of sugar species were determined based on the concept of free energy parameter. The model has been validated against an experimental data set derived from an apple juice concentration process and shows accepted relative errors between theoretical and experimental results for most operating parameters. The model has been used for further simulation to study the influence of various operating conditions on permeate flux and aroma compounds rejection. Further work is planned to optimize the apple juice concentration and aroma compound retention by assessing the impact of module area and operating variables.

References

Álvarez V., Álvarez S., Riera F., and Álvarez R., 1997. Permeate flux prediction in apple juice concentration by reverse osmosis. Journal of Membrane Science, 127, 25-34.

Álvarez S., Riera F., Álvarez R. and Coca J., 1998. Permeation of apple juice compounds in reverse osmosis. Separation Purification Technology, 14, 209-220.

Álvarez S., Riera F., Álvarez R. and Coca J., 2001. Prediction of flux and aroma compounds rejection in a reverse osmosis concentration of apple juice model solutions. Ind. Eng. Chem. Res., 40, 4925-4934.

Álvarez S., Riera F., Álvarez R. and Coca J., 2002. Concentration of apple juice by reverse osmosis at laboratory and pilot-plant scales. Ind. Eng. Chem. Res., 41, 6156-6164.

556 Cheong K. W.,Tan C. P., Mirhosseini H., Abdul Hamid N. S., Osman A. and Basri M., 2010.
557 Equilibrium headspace analysis of volatile flavor compounds extracted from soursop
558 (Annona muricata) using solid-phase microextraction. Food Research International,
559 43(5), 1267-1276.

560 Dickson J. M., Matsuura T., Blais P. and Sourirajan S., 1975. Reverse osmosis separation in
561 some organic and inorganic solutes in aqueous solutions using aromatic polyamide
562 membranes. Journal of Applied Polymer Science, 19, 801-819.

563 Gladdon J. K. and Dole M., 1953. Diffusivity determination of sucrose and glucose solutions.
564 J. Am. Chem. Soc., 75, 3900-3904.

565 Constenla D. T., Lozano J. E. and Crapiste G. H., 1989. Thermo-physical properties of
566 clarified apple juice as a function of concentration and temperature. J. Food Sci., 54(3),
567 663-668.

568 Girard B. and Fukumoto L. R., 2000. Membrane processing of fruit juices and beverages: A
569 review. Critical Reviews in Food Science and Nutrition, 40(2), 91-157.

570 Jain S. and Gupta S. K., 2004. Analysis of modified surface force pore flow model with
571 concentration polarization and comparison with Spiegler–Kedem model in reverse
572 osmosis systems. Journal of Membrane Science, 232(1-2), 45-62.

573 Jiao B., Cassano A. and Drioli E., 2004. Recent advance on membrane processes for the
574 concentration of fruit juices: A review. Journal of Food Engineering, 63, 303-324.

575 Lee C., Chen Y. and Wang G., 2010. A dynamic simulation model of reverse osmosis
576 desalination systems. The 5th International Symposium on Design, Operation and
577 Control of Chemical Processes, PSE Asia, Singapore.

578 Lonsdale H. K., Merten U. and Riley R. L., 1965. Transport properties of cellulose acetate
579 osmotic membranes. Journal of Applied Polymer Science, 9, 1341-1362.

580 Malalyandi P., Matsuura T. and Sourirajan S., 1982. Predictability of membrane performance
581 for mixed solute reverse osmosis systems. System cellulose acetate membrane-D-
582 Glucose-D,L-Malic acid-water. Ind. Eng. Chem. Process. Dev., 21, 277-282.

583 Matsuura T., Bednas M. E., Dickson J. M. and Sourirajan S., 1974. Polar and steric effects in
584 reverse osmosis. Journal of Applied Polymer Science, 18, 2829-2846.

585 Matsuura T., Bednas M. E., Dickson J. M. and Sourirajan S., 1975. Reverse osmosis
586 separations of aldehydes, ketones, and ethers in aqueous solutions using porous
587 cellulose acetate membranes. J. Appl. Polym. Sci., 19(9), 2473-2484.

588 Matsuura T., Dickson J. M. and Sourirajan S., 1976. Free energy parameters for reverse
589 osmosis separations of undissociated polar organic solutes in dilute aqueous solutions.
590 Ind. Eng. Chem. Process Des. Dev., 15(1), 149-161.

591 Nabetani H., Nakajima M., Watanabe A., Ikeda S., Nakao S. and Kimura S., 1992a.
592 Development of a new type of membrane osmometer. Journal of Chemical Engineering
593 of Japan, 25, 269-274.

594 Nabetani H., Nakajima M., Watanabe A., Nakao S. and Kimura S., 1992b. Prediction of the
595 flux for the reverse osmosis of a solution containing sucrose and glucose. Journal of
596 Chemical Engineering of Japan, 25(5), 575-580.

597 Pereira E. N., Matsuura T. and Sourirajan S., 1976. Reverse osmosis separations and
598 concentrations of food sugars. J. Food Sci., 41, 672.

599 Pepper D., 1990. RO for improved products in the food and chemical industries and water
600 treatment. Desalination, 77, 55-71.

601 Pozderovic´ A., Moslavac T. and Pichler A., 2006. Concentration of aqueous solutions of
602 organic components by reverse osmosis II. Influence of transmembrane pressure and
603 membrane type on concentration of different alcohol solutions by reverse osmosis.
604 Journal of Food Engineering, 77, 810-817.

605 Process System Enterprise Ltd, 2001. gPROMS Introductory User Guide. Process System
606 Enterprise Ltd., London.

607 Sheu M. and Wiley R., 1983. Preconcentration of apple juice by reverse osmosis. Journal of
608 Food Science, 48(2), 422-429.

609 Schock G. and Miquel A., 1987. Mass transfer and pressure loss in spiral wound modules.
610 Desalination, 64, 339-352.

611 Wilke C. R. and Chang P., 1955. Correlation of diffusion coefficients in dilute solutions.
612 A.I.Ch.E. Journal, 1(2), 264-270.

613

614

615

616 Table 1: Characteristics of the sugar and aroma compounds and their inlet concentration in the model solution of
617 10.5 °Brix (Matsuura et al., 1976; Álvarez et al., 1998; Malalyandi et al., 1982; Álvarez et al., 2002)

Compound	Molecular weight M_{wt}, (kg/kmol)	Concentration $C_{b(0)}$, (kmol/m³)	Molar volume, $V_{bp,A}$ (m³/kmol)	Free energy parameter, $(-\frac{\Delta\Delta G}{RT})_{25\,°C}$	Steric Taft number, $(\delta^{*}Es^{*})_{25\,°C}$	Solute transport parameter, $B_{s,25\,°C}$ (m/s)
sucrose	342	0.035555	0.215689	-1.76	-7.42	2.32996E-10
glucose	180	0.138000	0.116987	1.81	-5.42	6.11461E-8
malic acid	134	0.029104	0.083337	---	---	5.40E-8
fructose	180	0.340722	0.106351	1.59	-5.56	4.26602E-8
sorbitol	182	0.018406	0.122343	1.82	-5.57	5.31579E-8
ethyl acetate	88.11	0.000566	0.097683	2.11	-0.07	4.818E-6
ethyl butanoate	116.16	0.000129	0.132150	1.54	-0.43	1.739E-6
ethyl-2-methyl butanoate	130.19	5.37E-05	0.150508	1.47	-1.20	0.223E-6
isopentyl acetate	130.19	0.000130	0.148618	1.47	-0.35	0.387E-6
Hexyl acetate	144.22	6.926E-05	0.166274	1.85	-0.40	1.564E-6
trans-2-hexenal	98.143	0.000712	0.116004	---	---	4.574E-6
hexanal	100.2	0.000149	0.123095	2.19	-0.40	2.084E-6
isobutanol	74.12	0.000269	0.092421	2.42	-0.93	0.302E-6
butanol	74.12	0.000269	0.091506	2.17	-0.39	1.905E-6
isopentanol	88.15	0.000169	0.108771	2.12	-0.35	0.297E-6
hexanol	102.18	0.000293	0.125522	2.81	-0.40	1.556E-6

618

619 Table 2: Specifications of the spiral-wound membrane element (Álvarez et al., 2002)

Make	***Sparem Spa. (Biella, Italy)***
Membrane type and configuration	MSCB 2521 R99, Spiral-wound, Polyamide membrane
Active surface area (m^2)	1.03
Feed and permeate spacer thickness (t_f) and (t_p) (m)	0.0007 and 0.00055
Membrane sheet length (L) and width (W) (m)	0.44 and 2.3409
Hydraulic diameter (m)	0.00096
Max. operating pressure (atm)	41.4508
Max. operating temperature (°C)	50

620

621

622

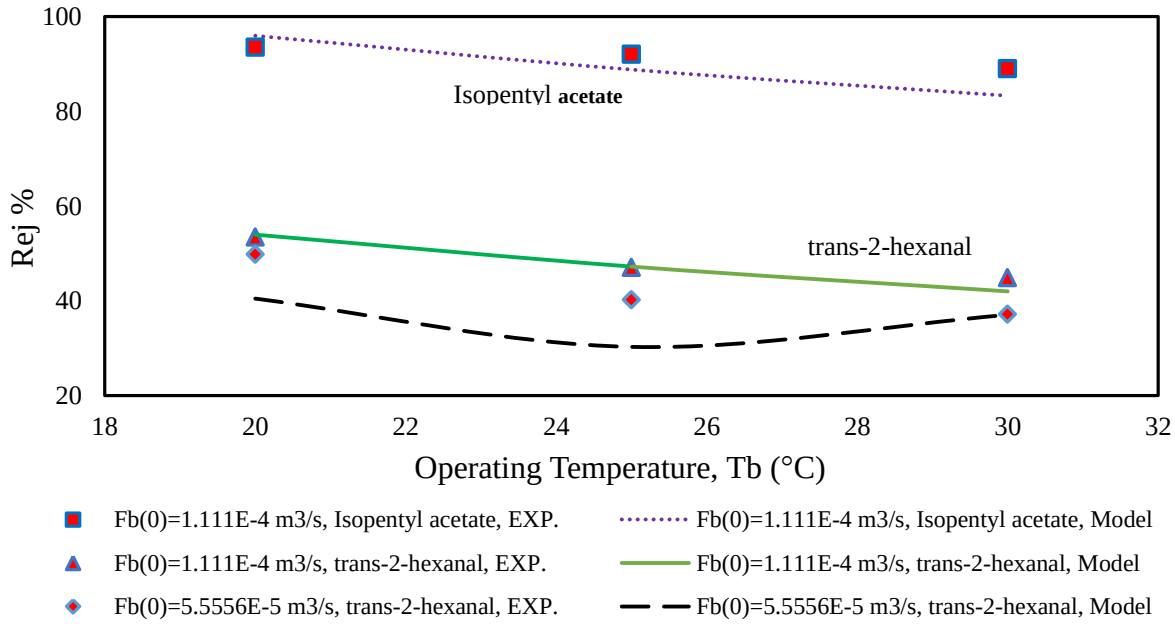

Figure 1: Experimental and model rejections of the two selected aroma compounds versus average operating temperature for two different inlet feed flow rates at inlet conditions (°Brix = 10.5, $TMP = 34.542$ atm)

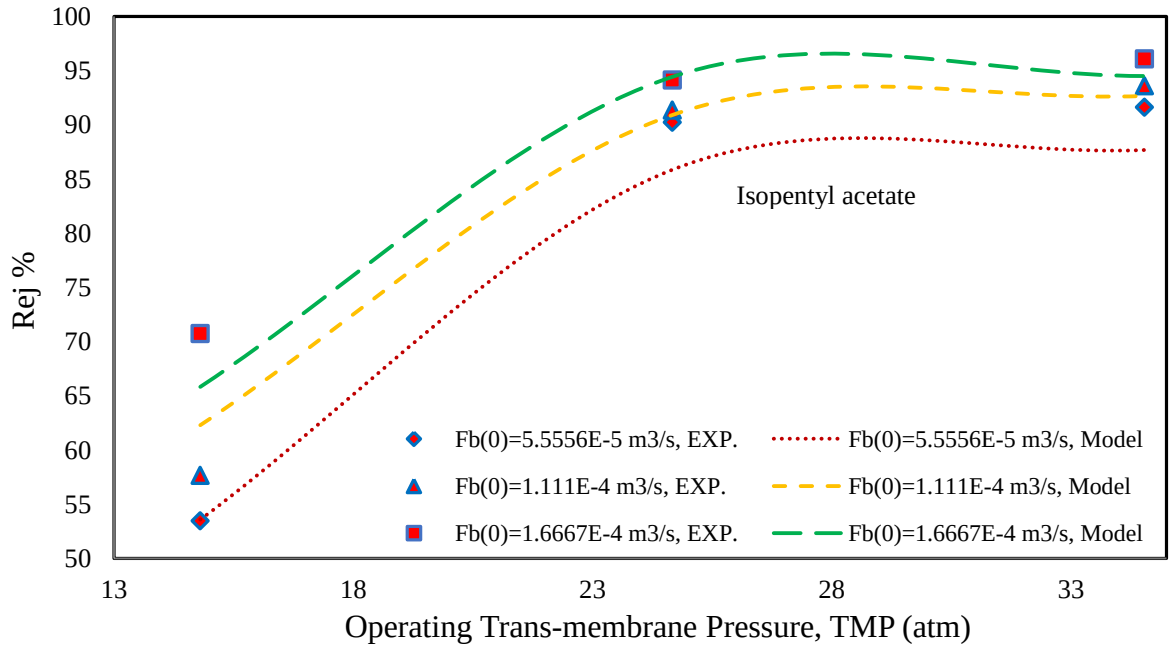

Figure 2: Experimental and model Isopentyl acetate rejection versus operating trans-membrane pressure for three different inlet feed flow rates at inlet conditions (°Brix = 10.5, $T_b = 20$ °C)

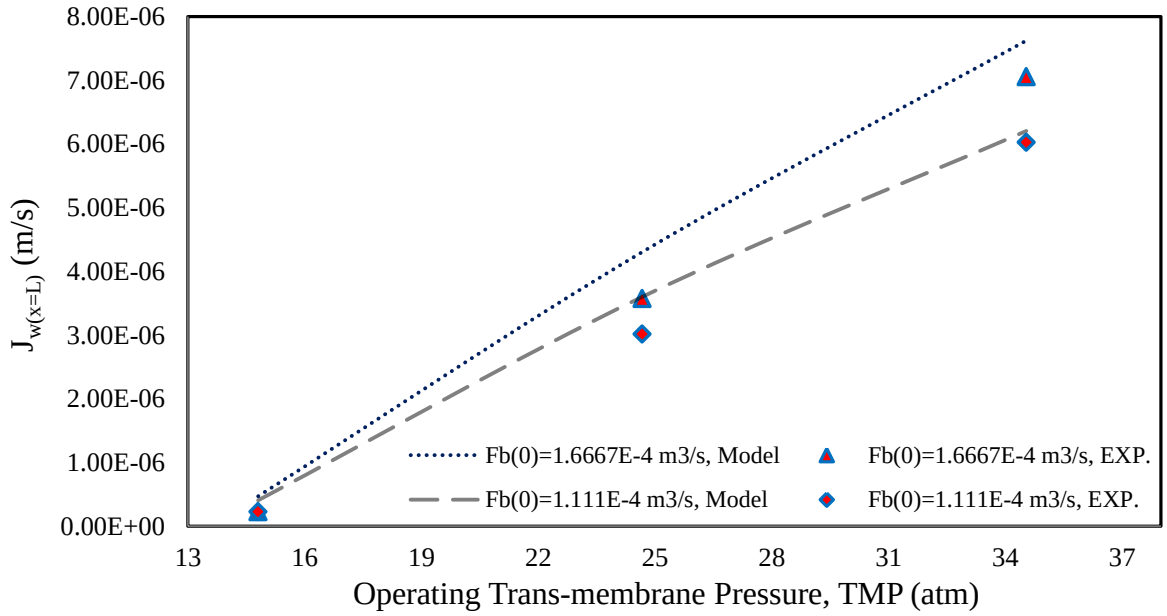

Figure 3: Experimental and model outlet water flux versus operating trans-membrane pressure for two different inlet feed flow rates at inlet conditions (°Brix = 10.5, T_b = 20 °C)

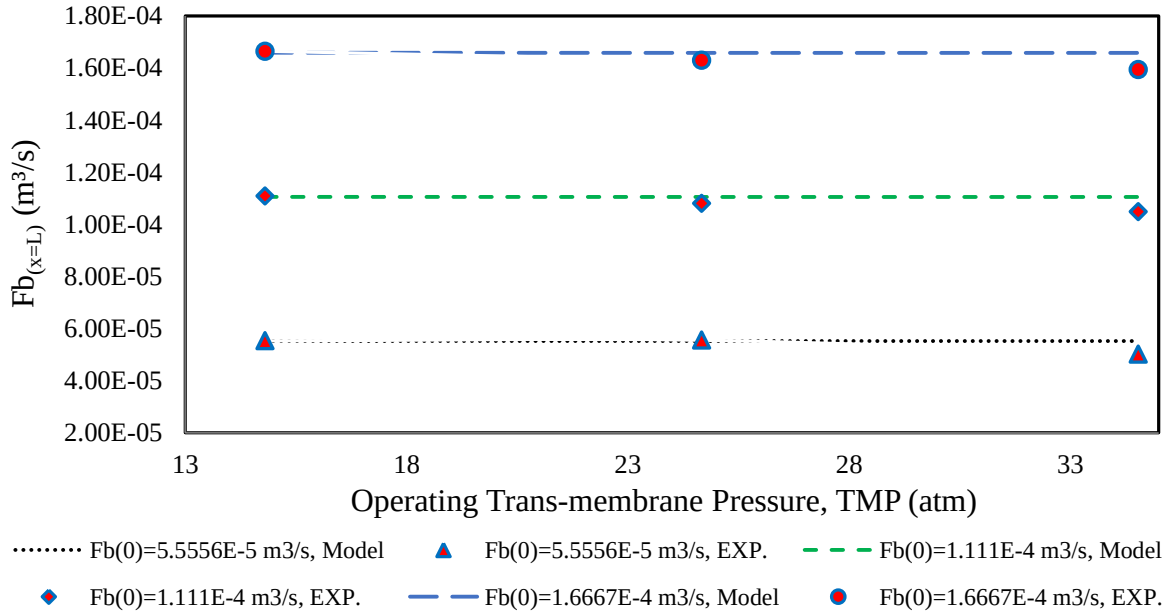

Figure 4: Experimental and model outlet feed flow rate versus operating trans-membrane pressure for three different inlet feed flow rates at inlet conditions (°Brix = 10.5, T_b = 20 °C)

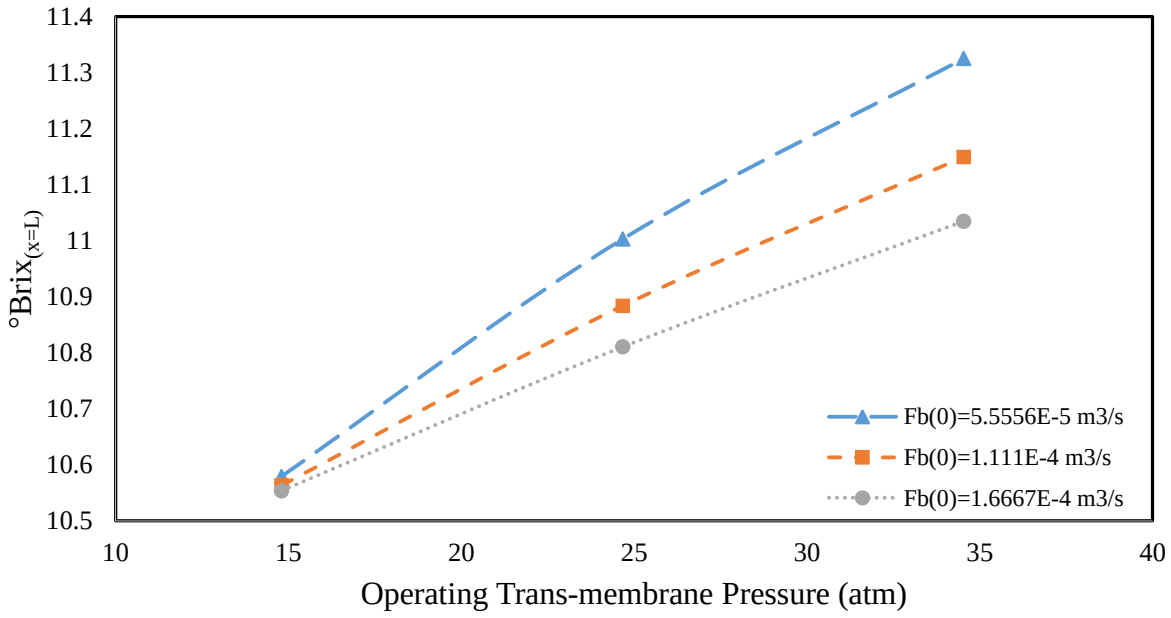

Figure 5: Outlet Brix variation as a function of operating trans-membrane pressure at different inlet feed flow rates at inlet conditions (°Brix = 10.5, $T_b = 20$ °C)

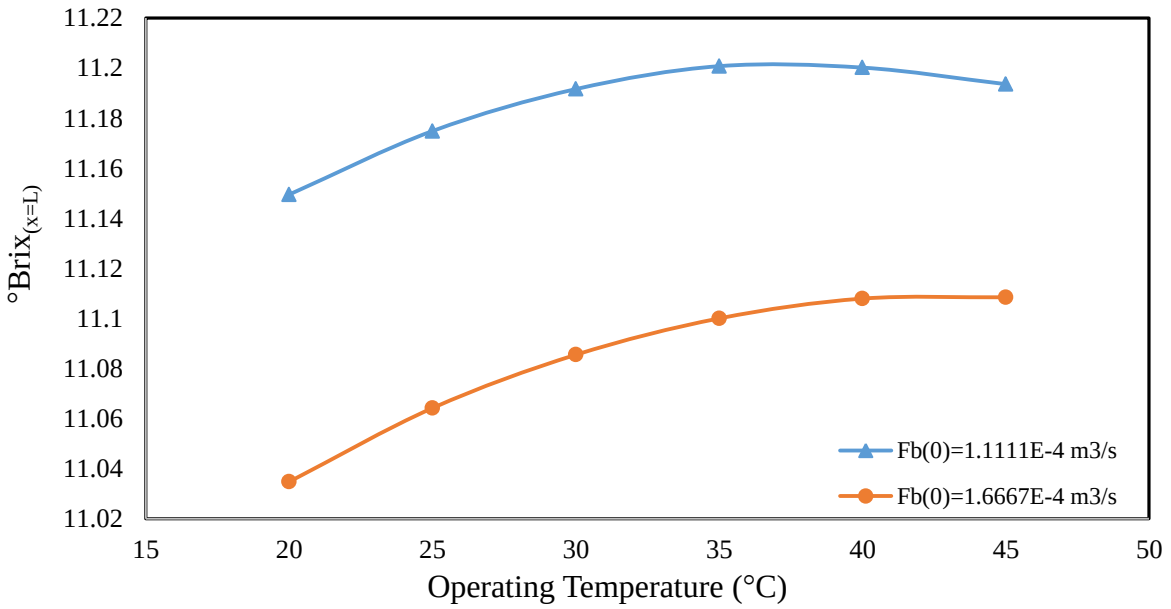

Figure 6: Outlet Brix variation as a function of operating temperature at different inlet feed flow rates at inlet conditions (°Brix = 10.5, $TMP = 34.542$ atm)

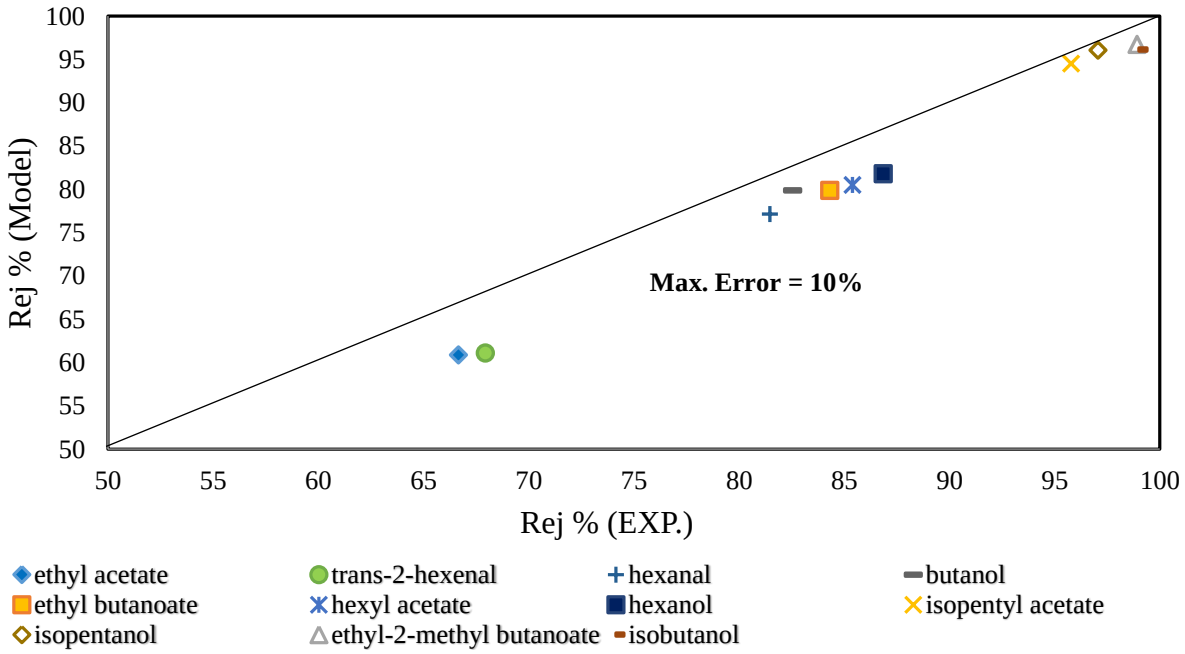

Figure 7: Experimental and predicted aroma compounds rejection at inlet conditions (°Brix = 10.5, T_b = 20 °C, TMP = 34.542 atm, $F_{b(0)}$ = 1.6667E-4 m³/s)